Earth Syst. Dynam. Discuss., 3, 935–977, 2012
www.earth-syst-dynam-discuss.net/3/935/2012/
doi:10.5194/esdd-3-935-2012
© Author(s) 2012. CC Attribution 3.0 License.

Earth System Dynamics Discussions

This discussion paper is/has been under review for the journal Earth System Dynamics (ESD). Please refer to the corresponding final paper in ESD if available.

The impact of model variation in CO_2 and temperature impulse response functions on emission metrics

D. J. L. Olivié[1,2] **and G. P. Peters**[1]

[1]Center for International and Environmental Climate Research – Oslo (CICERO), Oslo, Norway
[2]Department of Geosciences, University of Oslo, Oslo, Norway

Received: 30 July 2012 – Accepted: 9 August 2012 – Published: 3 September 2012

Correspondence to: D. J. L. Olivié (dirk.olivie@geo.uio.no)

Published by Copernicus Publications on behalf of the European Geosciences Union.

Abstract

Emission metrics are necessary to determine the relative climate effect of emissions of different species, such as between CO_2 and CH_4. Most emission metrics are based on Impulse Response Functions (IRFs) derived from singe models. There is currently very little understanding on how IRFs vary across models, and how the model spread propagates into the metric values. In this study, we first derive three CO_2 IRF distributions from Carbon-Cycle models in the inter-comparison projects C^4MIP and LTMIP, and three temperature IRF distributions from AOGCMs in the inter-comparison projects CMIP3 and CMIP5. Each distribution is based on the behaviour of several models, and takes into account their spread. The derived IRF distributions differ considerably, which is partially related to differences among the underlying models, but also to the specific scenarios (experimental setup) used in the inter-comparison exercises. For example, the very high emission pulse in LTMIP leads to considerably higher CO_2 IRFs, while the abrupt forcing scenario in CMIP5 leads to a relatively high temperature IRF the first four to five years. The spreads within the different IRF distributions are however rather similar. In a second part of the study, we investigate how differences among the IRFs then impact GWP, GTP and iGTP emission metric values for time horizons up to 100 yr. The spread in the CO_2 IRFs causes rather similar impacts in all three metrics. The LTMIP IRF gives 20–35 % lower metric values, while the C^4MIP IRFs give up to 40 % higher values for short time horizons shifting to lower values for longer time horizons. Within each derived CO_2 IRF distribution, underlying model differences give similar spreads on the metrics in the range of −15 % to 25 % (10–90 % spread). The GTP and iGTP metrics are also impacted by spread in the temperature IRFs, and this impact differs strongly between both metrics. For GTP, the impact of the spread is rather strong for species with a short life time. For BC, depending on the time horizon, 50 % lower to 85 % higher values can be found using the CMIP5 IRF, and slightly lower variations are found when using the CMIP3 IRFs (10 % lower to 40 % higher). For CH_4 the impact from spread in the temperature IRF is still considerable, but it becomes small for

ESDD
3, 935–977, 2012

longer-lived species. On the other hand, the impact from spread in the temperature IRF on iGTP is very small for all species for time horizons up to 100 yr as it is an integrated metric. Finally, as part of the spread in IRFs is caused by the specific setup of the inter-comparison exercises, there is a need for dedicated inter-comparison exercises to derive CO_2 and temperature IRFs.

1 Introduction

Comparing the global climate impact of the emission of various species, requires emission metrics such as Global Warming Potential (GWP), Global Temperature change Potential (GTP), and Integrated Global Temperature change Potential (iGTP). These metrics compare the impact of the pulse emission of a certain species with the impact of the pulse emission of the same amount of carbon dioxide (CO_2). GWP compares the radiative forcing (RF) integrated from the time of emission until a specified time, the so-called time horizon (Houghton et al., 1990); GTP compares the instantaneous global-mean temperature impact at a certain time after the emission (Shine et al., 2005); iGTP compares the temperature impact integrated from the time of emission until a time horizon (Peters et al., 2011). Frequently used metrics are GWP at time horizons of 20, 100, or 500 yr (yr), and GTP at time horizons of 20, 50, or 100 yr (Fuglestvedt et al., 2003; Shine et al., 2005, 2007; Fuglestvedt et al., 2010). Analytical expressions for emission metrics are usually based on Impulse Response Functions (IRFs). The IRFs are calibrated against more complex models, i.e., Carbon Cycle (CC) models to find the CO_2 IRF and Atmosphere Ocean General Circulation Models (AOGCMs) to find the temperature IRF.

A CO_2 IRF describes how the CO_2 excess atmospheric burden after the emission of a certain amount of CO_2 evolves as a function of time. After the emission, CO_2 will be removed from the atmosphere by uptake through vegetation and the ocean. Part of the CO_2 is taken up on relatively short time scales, but part will remain in the atmosphere for very long time (1000–100000 yr) (Archer et al., 2009). IRFs due to their

ESDD
3, 935–977, 2012

inherent linear nature can not capture the non-linearities which are clearly present in the CO_2 system (Joos et al., 1996). As the atmospheric CO_2 mixing ratio rises and the upper ocean becomes saturated in CO_2 (limited buffer capacity of the ocean mixed layer), the ocean is less able to take up CO_2 (Caldeira and Kasting, 1993) until ocean circulation moves carbon into the deeper ocean. Also through the vegetation uptake non-linearities exist as a higher CO_2 atmospheric mixing ratio is assumed to increase fertilization (negative feedback) (Friedlingstein et al., 2006). Further non-linearities are present through the ocean circulation, the temperature dependence of CO_2 solubility in the ocean, CO_2 fertilization (higher temperature reduces the CO_2 uptake by vegetation), but also precipitation changes (indirect). Some of these non-linearities were investigated by Gillett and Matthews (2010) in relation to metric values. One of the important consequences is that IRFs for CO_2 are dependent on the size of the emission pulse (Hooss, 2001; Eby et al., 2009). CO_2 uptake is also dependent on the emissions of nitrogen oxides (NO_x) and Volatile Organic Compounds (VOCs) through the negative impact of ozone (O_3) on the CO_2 uptake by vegetation (Sitch et al., 2007; Collins et al., 2010).

Also for non-CO_2 species, IRFs are used to describe the atmospheric burden after their emission. The IRFs for non-CO_2 species are usually based on a single time scale, i.e. the life time. This life time can vary different orders of magnitude among species, from a few days for black carbon aerosol (BC) until thousands of years for sulfur hexafluoride (SF_6).

To convert the CO_2 IRF, or that of other species, into radiative forcing requires an estimate of the radiative efficiency, i.e., the marginal increase in RF as a function of the atmospheric mixing ratio (IPCC, 2007). Non-linearities exist, for example, due to the saturation of spectral absorption bands (e.g. for CO_2) or due to the overlap of spectral absorption bands for different species, e.g. between methane (CH_4) and nitrous oxide (N_2O) (see the expressions of the RF for CO_2, CH_4 and N_2O in IPCC (2001)). Due to the non-linear dependency of the RF on the CO_2 mixing ratio, the background mixing ratio of the species and the size of the emission pulse impact the specific RF.

ESDD
3, 935–977, 2012

IRFs are also used to describe the global-mean temperature response of the Earth's System to radiative forcings (Hasselmann et al., 1993; Sausen and Schumann, 2000). A temperature IRF describes the response to a δ-pulse radiative forcing (the size of this pulse forcing is such that its time-integrated value is $1\,W\,m^{-2}\,yr = 31.6 \times 10^6\,J\,m^{-2}$). A more physical interpretation is obtained when integrating the IRF, which describes then the response to a step increase in RF. When modelled in an AOGCM, the global-mean temperature response of the Earth's System to a RF shows a fast response determined by the atmosphere, the ocean mixed layer and the land surface, and slower responses which reflect the adaptation of the deeper ocean. Using two time constants describes the AOGCM temperature evolution response to a RF reasonably well (Boucher and Reddy, 2008; Li and Jarvis, 2009; Olivié and Stuber, 2010; Olivié et al., 2012), while one time constant often gives a too crude description (Shine et al., 2005; Gillett and Matthews, 2010; Olivié et al., 2012). The important role of the slow mode for the atmospheric response is clearly shown by Held et al. (2010) in a specific AOGCM experiment.

One must be aware, however, that an accurate representation of the Earth's System temperature response by IRFs might be hampered by non-linearities in the ocean. Manabe and Stouffer (1994) found a very different behaviour of the Atlantic Meridional Overturning Circulation in AOGCM experiments with a doubling or quadrupling of the CO_2 mixing ratio. In addition, there is an asymmetry between heating and cooling time scales in the ocean, i.e., the ocean response to surface cooling could be twice as fast as to surface warming (Stouffer, 2004; Yang and Zhu, 2011). These non-linearities cannot be reproduced by IRFs. The derivation of IRFs also suffers from the fact that AOGCM simulations are computationally expensive, and rather few very long integrations with AOGCMs exist, thus hampering the estimation of the slow time scale. Stouffer (2004), Danabasoglu and Gent (2009), and Yang and Zhu (2011) indicate that the equilibrium timescale of the ocean can be much larger than 1000 yr, but a large majority of AOGCM simulation has a length of only 100–300 yr (e.g., CMIP3 and CMIP5), leaving large uncertainties on the temperature evolution on large time scales.

ESDD
3, 935–977, 2012

Although IRFs have their limitations of which some are described above, they are widely used. IPCC (2007) used a CO_2 IRF based on an updated version of the Bern CC-model (Bern2.5CC, Joos et al. (2001)), and several recent studies use the temperature IRF from Boucher and Reddy (2008) based on a simulation with the UKMO-HadCM3 AOGCM. These two IRFs are based on the behaviour of only one parent model, and in addition combining them in the GTP and iGTP metric may be inconsistent. In recent years, many idealized simulations with CC-models and AOGCMs have become available in inter-comparison projects, and can be used to derive IRFs. The behaviour of these models differs considerably, and we investigate the spread in the IRFs. We then use these derived IRFs to calculate GWP, GTP and iGTP metrics, and quantify how they are influenced by the spread in the IRFs. Our work is comparable with Reisinger et al. (2010) who presented uncertainty estimates for emission metrics of CO_2 and CH_4, using a Simple Climate Model (SCM) calibrated on CMIP3 AOGCM results and C^4MIP CC-model results (partially using results from OCMIP2). With respect to their study, we study more species (also BC, N_2O and SF_6), and use data from more recent inter-comparison projects (LTMIP and CMIP5).

The structure of the paper is as follows. In Sect. 2, we describe emission metrics and IRFs. In Sect. 3, we describe the data and method we use to derive IRFs. In Sect. 4, we present the derived IRFs, and the impact of the spread in IRFs on emission metrics. In Sect. 5, we present our conclusions.

2 Emission metrics and IRFs

2.1 IRFs

IRFs are a condensed way to describe the atmospheric burden of species as a function of their emissions, or the evolution of the global-mean temperature in response to a radiative forcing.

ESDD
3, 935–977, 2012

2.1.1 Burden IRFs

The atmospheric burden evolution after the pulse emission of 1 kg of a species X is often written as a sum of decaying exponential functions (modes),

$$\mathrm{IRF}_X(t) = \sum_{i=0}^{n-1} a_i \exp\frac{-t}{\tau_i}, \quad (1)$$

with

$$\sum_{i=0}^{n-1} a_i = 1. \quad (2)$$

The atmospheric burden $B(t)$ in response to any emission scenario $E(t)$ can than be written as the convolution integral

$$B(t) = (E \otimes \mathrm{IRF}_X)(t) \equiv \int_0^t E(t')\,\mathrm{IRF}_X(t-t')\,\mathrm{d}t'. \quad (3)$$

For BC, CH_4, N_2O and SF_6 one usually limits the expression to one mode, where the then unique τ in Eq. (1) then represents the life time of the species. BC emissions disappear on average within a week, while CH_4, N_2O and SF_6 have life times of around 12, 114, and 3200 yr, respectively (see Table 1). This description is a simplified method as the burden evolution does not appear to depend on the location or timing of the emission. It is a good approximation for the relatively well mixed species CH_4, N_2O and SF_6, but rather crude for BC due to the combination of a short life time and a heterogeneous geographical distribution of its removal.

For the emission of CO_2, the situation is more complicated. Part of its emission disappears fast from the atmosphere on a time scale of 1 to 10 yr, while a substantial part remains in the atmosphere for much longer time. One mode is insufficient to describe the atmospheric CO_2 burden evolution after a pulse emission (Archer et al., 2009). A

ESDD
3, 935–977, 2012

best estimate for the evolution of CO_2 used in IPCC (2007) is an expression with four modes ($n = 4$ in Eq. 1), and the corresponding values of a_i and τ_i are given in the upper row of Table 3. Notice that $\tau_0 = \infty$, indicating that 21.7 % of the emission amount ($a_0 = 0.217$) is assumed to stay perpetually in the atmosphere.

If one additionally assumes that the RF is a linear function of the atmospheric burden, one can easily express the evolution of the RF as a function of time. This is not completely true for CO_2 where the RF shows a logarithmic dependence on its burden, or for N_2O and CH_4 due to a mutual impact (IPCC, 2001). However, a linear approximation can be used when assuming a small perturbation around a well-defined reference state. Approximate values for the specific radiative forcing of different species are given in Table 1. The specific radiative forcing of CO_2 (see Table 1) is based on the radiative forcing expression for CO_2 in IPCC (2001), assuming a background mixing ratio of 378 ppmv (IPCC, 2007).

2.1.2 Temperature IRF

IRFs can also be used to express approximatively the temperature evolution in response to a specified radiative forcing. Based on AOGCM results, expressions for the expected global-mean temperature change $T(t)$ due to a radiative forcing can be approximately described by a convolution integral o f the radiative forcing $\mathrm{RF}(t)$ with a temperature IRF $\mathrm{IRF}_T(t)$,

$$T(t) = (\mathrm{RF} \otimes \mathrm{IRF}_T)(t) \equiv \int_0^t \mathrm{RF}(t')\,\mathrm{IRF}_T(t - t')\,\mathrm{d}t' . \quad (4)$$

The temperature IRF is often described as a sum of decaying exponential functions,

$$\mathrm{IRF}_T(t) = \sum_{i=1}^{n} \frac{f_i}{\tau_i} \exp\frac{-t}{\tau_i} . \quad (5)$$

ESDD
3, 935–977, 2012

This function describes the evolution of the global-mean temperature change after a δ-pulse radiative forcing, where the forcing felt by the system is equivalent to a forcing of $1\,\mathrm{W\,m^{-2}}$ during 1 yr. For a RF scenario that jumps at $t = 0$ from 0 to $1\,\mathrm{W\,m^{-2}}$ and remains constant at that value for $t > 0$, one finds, using Eqs. (4) and (5), that the temperature evolution $T(t)$ can be written as

$$T(t) = \sum_{i=1}^{n} f_i \left(1 - \exp\frac{-t}{\tau_i}\right). \quad (6)$$

This shows that the sum of the f_i in the IRF can be interpreted as the climate sensitivity, i.e. $\lambda = \sum_{i=1}^{n} f_i$ (taking $t \to \infty$ in Eq. 6). In the literature, one finds as well expressions with $n = 1$ (Hasselmann et al., 1993), $n = 2$ (Boucher and Reddy, 2008) as $n = 3$ (Li and Jarvis, 2009). A frequently used expression with $n = 2$ is the one presented in Boucher and Reddy (2008), and the corresponding values of f_i and τ_i are given in the upper row of Table 4. For expressions with $n \geq 2$, the fast mode represents the fast response of the atmosphere, the land-surface, and the ocean mixed layer, while the other mode(s) represent(s) the slow response of the ocean.

2.2 Emission metrics

Emission metrics are one of the tools to quantify and compare the impact of the emissions of different species. The expressions for the burden IRF and temperature IRF presented above, can then be used to calculate several metrics.

The absolute global warming potential (AGWP) of a certain species is the time-integrated RF caused by the emission of 1 kg of that species,

$$\mathrm{AGWP}_X(H) = \int_0^H A_X\,\mathrm{IRF}_X(t)\,\mathrm{d}t, \quad (7)$$

with H the time horizon, A_X the radiative efficiency of species X (see Table 1), and $\mathrm{IRF}_X(t)$ the burden IRF (see Eq. 1). The undimensional GWP of a species is the AGWP

ESDD
3, 935–977, 2012

of that species divided by the AGWP of CO_2,

$$\mathrm{GWP}_X(H) = \frac{\mathrm{AGWP}_X(H)}{\mathrm{AGWP}_{\mathrm{CO}_2}(H)}. \quad (8)$$

The GWP metric has been used extensively last two decades to compare the climate effect of various species. Typical time horizons are 20, 100, and 500 yr, though 100 yr is most common due to its application in the Kyoto Protocol.

By combining the burden IRF and the temperature IRF, one can express the global-mean temperature response due to the emission of a species. The absolute global temperature change potential (AGTP) indicates the impact of the emission of 1 kg of a certain species on the global-mean temperature at a certain time,

$$\mathrm{AGTP}_X(H) = \int_0^H A_X \,\mathrm{IRF}_X(t)\,\mathrm{IRF}_T(H-t)\,\mathrm{d}t, \quad (9)$$

with $\mathrm{IRF}_T(t)$ the temperature IRF (see Eq. 5). The undimensional GTP of a species is the AGTP of that species divided by the AGTP of CO_2,

$$\mathrm{GTP}_X(H) = \frac{\mathrm{AGTP}_X(H)}{\mathrm{AGTP}_{\mathrm{CO}_2}(H)}. \quad (10)$$

The integrated absolute temperature change potential (iAGTP) is the time-integral of AGTP,

$$\mathrm{iAGTP}_X(H) = \int_0^H \mathrm{AGTP}_X(t)\,\mathrm{d}t. \quad (11)$$

The undimensional iGTP of a species is the iAGTP of that species divided by the iAGTP of CO_2,

$$\mathrm{iGTP}_X(H) = \frac{\mathrm{iAGTP}_X(H)}{\mathrm{iAGTP}_{\mathrm{CO}_2}(H)}. \quad (12)$$

ESDD
3, 935–977, 2012

In addition to the dependence of (A)GTP and i(A)GTP on characteristics of the species (and eventually CO_2), they also depend on characteristics of the climate system.

3 Method and data

To obtain estimates for CO_2 IRFs and temperature IRFs, we use results from more complicated models. As we are interested in possible uncertainties in emission metrics, we focus on data from inter-comparison projects with different models participating in the same experimental setup. We will take into account the spread in their results, and see how that affects the metric values.

3.1 Data

For deriving both CO_2 and temperature IRFs, we use results from four different inter-comparison projects, and in this section we shortly describe these data. An overview of some of the characteristics of the inter-comparison projects can be found in Table 2. We will also shortly describe the data on which the reference CO_2 IRF (IPCC, 2007) and temperature IRF (Boucher and Reddy, 2008) are based.

3.1.1 IPCC (2007)

The CO_2 response function which has been used in IPCC (2007), is based on a 1000 yr-long simulation with the Bern CC-model (Bern2.5CC; Joos et al. (2001)). In that simulation, a background CO_2 mixing ratio of 378 ppm and a pulse emission of 40 Gt[C] were used. We will refer to this data set and IRF derived from it as J07.

3.1.2 C^4MIP

The C^4MIP (Coupled Climate Carbon Cycle Model Inter-comparison Project) experiments have been performed simulating the 1860–2100 period (a few models started

ESDD
3, 935–977, 2012

somewhat earlier or later) with coupled climate-CC-models (Friedlingstein et al., 2006). For the anthropogenic CO_2 emissions, observed values have been used up to around year 2000 and SRES scenario A2 values for the 21st century (Nakicenovic et al., 2000). The annual emissions increase from ~1 Gt[C] yr^{-1} in 1900, to ~8 Gt[C] yr^{-1} in 2000 and ~30 Gt[C] yr^{-1} in 2100.

Eleven coupled climate-CC-models participated in this inter-comparison exercise of which 7 are AOGCMs and 4 are models of intermediate complexity. These models are BERN-CC, CSM-1, CLIMBER2-LPJ, FRCGC, HadCM3LC, IPSL-CM2C, LLNL, IPSL-CM4-LOOP, MPI, UMD, and Uvic-2.7. A short description of these models can be found in Friedlingstein et al. (2006). Two different experiments were performed. In an uncoupled experiment (u) temperature feedbacks were not included, while in the coupled experiment (c) temperature feedbacks were included. All models indicated that a larger fraction of anthropogenic CO_2 stays airborne if temperature feedbacks are included. This comparison exercise was built on experiences from an earlier experiment including only two models (Cox et al., 2000; Dufresne et al., 2002; Friedlingstein et al., 2003).

3.1.3 LTMIP

A second data set we use to derive CO_2 IRFs is LTMIP (Long Tail Model Intercomparison Project) (Archer et al., 2009). The aim of this project was to quantify the long-term fate of fossil fuel CO_2 emissions in the atmosphere, ocean, and terrestrial biosphere. The participating groups performed 10000 yr-long simulations with CC-models, emitting CO_2 pulses of 1000 Gt[C] and 5000 Gt[C]. The pulse sizes are 1000 Gt[C] since mankind will likely surpass 1000 Gt[C] under business-as-usual projections by 2100 and 5000 Gt[C] as this is the estimated entire reservoir of fossil fuels (Archer et al., 2009). The reference state was an atmospheric mixing ratio of 286 ppmv CO_2.

Different simulations have been performed, differing by the feedbacks taken into account in the CC-models. These feedbacks are the climate feedback (changing ocean temperatures impact the solubility of CO_2 and changes in ocean circulation influence

ESDD
3, 935–977, 2012

the ventilation patterns), sediment feedback, weathering feedback and vegetation feedback (absorbtion of carbon into biomass and soil organic matter in response to changes in the atmospheric CO_2 mixing ratio or climate). We have used the results from the reference simulation with a 1000 Gt[C] pulse emission and no feedbacks – this is a simulation performed by most of the models. These models are CC_SED, CLIMBER-2, GENIE8, GENIE16, GEOCYC, LTCM, MESMO, MPI-UW, and UVIC-2.8. A short description of these models can be found in Archer et al. (2009) and Cao et al. (2009). With one of these models (UVIC-2.8), Eby et al. (2009) further illustrate that the time required to absorb anthropogenic CO_2 strongly depends on the total emission amount.

3.1.4 Boucher and Reddy (2008)

Boucher and Reddy (2008) present a temperature IRF, derived from a 1000 yr-long simulation with the UKMO-HadCM3 AOGCM. The scenario used shows a 2 % yr^{-1} increase in the CO_2 mixing ratio up to a quadrupling (reached after 70 yr), after which the CO_2 mixing ratio is kept constant. The temperature IRF of Boucher and Reddy (2008) contains two modes, with time constants of 8.4 and 409.5 yr. The values of f_i and τ_i can also be found in the top row of Table 4. Li and Jarvis (2009) used the same data but a different method to estimate the modes. Using two modes they find very similar values, and using three modes small differences in the integrated temperature IRF only show up after 500 yr.

3.1.5 CMIP3

The first set of AOGCM results we use to derive temperature IRFs is taken from the World Climate Research Programme's Coupled Model Inter-comparison Project phase 3 (CMIP3), which has been used for the IPCC Fourth Assessment Report (IPCC, 2007). Among the different simulations available from the CMIP3 exercise, we use the idealized experiments where the CO_2 mixing ratio increases by 1 % yr^{-1}, and is kept constant after 70 yr (doubling of CO_2) or after 140 yr (quadrupling of

ESDD
3, 935–977, 2012

CO_2). These are gradually changing scenarios, and have for most of the AOGCMs a length of 210–290 yr, but less than 100 yr for a few of them. The subset of 15 models we use consists of CGCM3.1(T47), CNRM-CM3, ECHO-G, FGOALS-g1.0, GFDL-CM2.0, GFDL-CM2.1, GISS-EH, GISS-ER, INM-CM3.0, IPSL-CM4, MIROC3.2(hires), MIROC3.2(medres), MRI-CGCM2.3.2 ,UKMO-HadCM3, and UKMO-HadGEM1. More information on these models can be found in IPCC (2007).

For the models used in this comparison exercise (except for CNRM-CM3) also the total climate sensitivity λ (see Sect. 2.1.2) has been estimated in IPCC (2007), based on an experiment where the Atmosphere General Circulation Models (AGCMs) alone were coupled to a Mixed Layer Ocean (MLO) model (IPCC, 2007). In one of the approaches we use the estimated climate sensitivity as an additional constraint, and we refer to that case as CMIP3*.

3.1.6 CMIP5

In the more recent CMIP5 exercise (Taylor et al., 2012) which will be used in the IPCC Fifth Assessment Report, the scenarios useful for the calibration of IRFs are a scenario with an instantaneous quadrupling of the CO_2 mixing ratio, and one with a gradual increase in CO_2 mixing ratio at a rate of $1\,\%\,yr^{-1}$ (without stabilization). The length of the simulations is 140–150 yr which is considerably shorter than the experiments in CMIP3.

We use the results from 15 models, i.e., CanESM2, CNRM-CM5, CSIRO-Mk3.6.0, GFDL-CM3, GFDL-ESM2G, GFDL-ESM2M, HadGEM2-ES, INM-CM4, IPSL-CM5A-LR, MIROC5, MIROC-ESM, MPI-ESM-LR, MPI-ESM-P, MRI-CGCM3, and NorESM1-M.

ESDD
3, 935–977, 2012

3.2 Method

In this section, we shortly describe how we estimate the parameters in the IRFs, how we construct the IRF distributions, and how we calculate the spread in the emission metrics.

3.2.1 Estimating the IRF parameters

For every CC-model and AOGCM in the data sets above, we have estimated the parameters in the IRFs of Eqs. (1) and (5), respectively. We use a CO_2 IRF with four modes (one of which is a constant term as we take $\tau_0 = \infty$), and a temperature IRF with two modes. To find the parameter values in the IRFs that best fit the behaviour of one single CC-model or AOGCM, we use an inverse modelling technique based on Tarantola (2005) and applied for SCMs in Olivié and Stuber (2010). It has been recently used on CMIP3 data (Olivié et al., 2012) to derive temperature IRFs, and here we apply it to derive both CO_2 and temperature IRFs. It optimizes the value of the CO_2 IRF parameters by minimising the difference between the CO_2 mixing ratio in the CC-model and the CO_2 mixing ratio obtained from the convolution of the CO_2 emission scenario with the CO_2 IRF, but also taking into account how much the IRF parameters deviate from some a priori values. Due to the condition that $\sum_{i=0}^{3} a_i = 1$ in the CO_2 IRF, we express the four a_i as a function of three parameters b_i which are related to the a_i by

$$a_0 = \frac{1}{1 + \sum_{j=1}^{3} b_j}, \tag{13}$$

and

$$a_i = \frac{b_i}{1 + \sum_{j=1}^{3} b_j} \quad (i = 1,2,3), \tag{14}$$

where $0 < b_i < \infty$ are now the parameters which have to be estimated. The temperature IRF parameters are optimized by minimizing the difference between the

ESDD
3, 935–977, 2012

temperature in the AOGCM and the temperature resulting from the convolution of the RF scenario with the temperature IRF, but also taking into account how much the IRF parameters deviate from some a priori values. We assume that all parameters (b_i, f_i, and τ_i) have a log-normal distribution, which guarantees that they remain positive. So for every single CC-model or AOGCM, we find a corresponding set of parameters which best reproduces its behaviour.

In principle, one can imagine a variety of numerical experiments with CC-models and AOGCMs, differing in the time evolution of the CO_2 emission $E(t)$ and the radiative forcing RF(t), respectively. Deriving an IRF from those experiments can be more or less difficult depending on the type of scenario. Ideal are experiments where the response of the CC-model or AOGCMs is already an IRF. This can be easily realized for the CC-models when using a pulse emission, as in J07 and LTMIP. However, for the temperature experiments, a δ-pulse experiment is difficult to realize, and therefore a step in the radiative forcing which is kept constant (as in CMIP5), or decays exponentially (Olivié and Stuber, 2010) is more common. For experiments which are not pulse experiments, deriving the IRF can be more complicated and one must be aware that the IRF cannot always be well determined.

3.2.2 IRF distribution

Once all the IRF parameter sets found, where each set best reproduces the behaviour of one CC-model or AOGCM, we group them together per inter-comparison project and derive a multivariate distribution for the parameters of the IRF – the distribution assumes that the logarithm of the parameters are normally distributed. This gives three CO_2 IRF distributions, based on C^4MIP(u), C^4MIP(c) and LTMIP data, respectively. When $\boldsymbol{x}$ is the vector consisting of the logarithm of the parameters of the CO_2 IRF,

$$\boldsymbol{x} = (\log\tau_1, \log\tau_2, \log\tau_3, \log b_1, \log b_2, \log b_3), \quad (15)$$

ESDD
3, 935–977, 2012

then the distribution of the parameters in the CO_2 IRF can be expressed as,

$$P(\boldsymbol{X} = \boldsymbol{x}) \sim \exp\left(-\frac{1}{2}(\boldsymbol{x} - \bar{\boldsymbol{x}})^T \boldsymbol{\Sigma}^{-1}(\boldsymbol{x} - \bar{\boldsymbol{x}})\right) \tag{16}$$

where

$$\bar{\boldsymbol{x}} = \frac{1}{n}\sum_{i=1}^{n} \boldsymbol{x}_i\,, \tag{17}$$

and

$$\boldsymbol{\Sigma} = \frac{1}{n-1}\sum_{i=1}^{n} (\boldsymbol{x}_i - \bar{\boldsymbol{x}})^T (\boldsymbol{x}_i - \bar{\boldsymbol{x}})\,. \tag{18}$$

The vector $\bar{\boldsymbol{x}}$ and the matrix $\boldsymbol{\Sigma}$ are estimates of the mean vector and the covariance matrix, respectively. The index i runs over all the CC-models (for n, see Table 2) in the specific inter-comparison exercise.

Similarly, three distributions for the parameters in the temperature IRF can be derived based on CMIP3, CMIP3*, and CMIP5 data, respectively, where the vector $\boldsymbol{x}$ now represents the parameters in the temperature IRF,

$$\boldsymbol{x} = (\log\tau_1, \log\tau_2, \log f_1, \log f_2)\,. \tag{19}$$

3.2.3 Monte-Carlo simulation

To calculate the GWP, GTP and iGTP emission metrics and their spread, we will use the CO_2 and temperature IRFs estimated from the CC-model and AOGCM results. We use these distributions to perform Monte-Carlo simulations to find distributions for GWP, GTP and iGTP. To obtain the GTP and iGTP distribution, one uses both CO_2 and temperature IRFs, and for simplicity, we assume that there is no correlation between the CO_2 IRF parameter values and the temperature IRF parameter values. The Monte-Carlo simulations consist of 20000 members. As the distribution is multivariate, this

ESDD
3, 935–977, 2012

necessitates that the covariance matrix is factorized as $\mathbf{\Sigma} = \mathbf{U}^T \mathbf{U}$ where $\mathbf{U}$ is an upper-triangular matrix.

4 Results

In this section we first describe the IRF distributions obtained by fitting the CC-model and AOGCM results. Then we describe the GWP, GTP and iGTP emission metric values we obtain for BC, CH_4, N_2O, and SF_6 for time horizons up to 100 yr (these species are chosen as they span a wide range of life times, i.e., 1 week, 12 yr, 114 yr, and 3200 yr, respectively).

4.1 IRFs

Figure 1 shows the principal results for the CO_2 IRFs. The left panel of Fig. 1 shows the CO_2 IRF for the reference J07 (black), and for the three distributions C^4MIP(u) (red), C^4MIP(c) (blue) and LTMIP (green) derived from the different inter-comparison exercises. The full lines indicate the median value, the dashed lines the 10- and 90-percentile values. The results based on LTMIP are significantly higher than the standard J07 CO_2 IRF. The 10-percentile estimate from LTMIP comes close to J07, and the estimate of the long term value is rather similar to the J07 value. The larger values in LTMIP are caused by the fact that the emission size was 1000 Gt[C], while the IRF in J07 was obtained using an emission pulse of 40 Gt[C]. Due to this very large amount, the ocean mixed layer is easily saturated inhibiting a faster take up of atmospheric CO_2.

The two IRFs based on C^4MIP give results different from J07 and LTMIP. The IRF shows initially a very fast decay (first year) followed by a much slower decay. This results in an atmospheric burden being greater than the value from J07 from year 30 onward – the value after 1000 yr being almost 60 to 100 % higher. One can also see that the results from the coupled experiment (c) give larger values for the IRF: the increasing temperature in the coupled experiment decreases the net CO_2 uptake, leaving

ESDD
3, 935–977, 2012

a larger fraction of CO_2 in the atmosphere. The large difference with respect to J07 is probably caused by the CO_2 emission scenario in C^4MIP. The near exponential increase in CO_2 emissions in this experiment makes it hard to estimate the IRFs. For such emission scenarios, different shapes of the IRFs can lead to exactly the same evolution of the CO_2 burden. This implies that if more than one mode must be estimated in the IRF, their weights and time scales can become indeterminate. However, as the emission scenario here is not exactly exponential, the experiment still contains additional information (Gloor et al., 2010) .

The right panel of Fig. 1 shows best estimates for the parameters of the four modes in the CO_2 IRF when calibrated to the individual CC-models. Every single dot corresponds with a tuple (τ_i, a_i) from Eq. (1) (the tuple (τ_0, a_0) with $\tau_0 = \infty$ is indicated at the right). The distributions of the CO_2 IRF obtained by combining the results within the same inter-comparison exercise are represented by the ellipses. The area within the ellipses covers 80 % of the distributions. Tilted ellipses indicate that there is some (anti-)correlation among the τ_i and a_i. There exist also correlations between the a_i and τ_i from different modes, but they are not represented in this figure. One can see that the LTMIP experiment gives parameters which are not very different from J07. However, C^4MIP(u) and C^4MIP(c) give values which are considerably different from J07: smaller values for the two small time constants τ_2 and τ_3, and higher values for τ_1. Also the contributions a_3 from the fastest mode and a_0 from the slowest mode are considerably larger.

Figure 2 shows the results for the temperature IRF with two modes. The top left panel shows the temperature IRF presented in Eq. (5). We have indicated the reference distribution from Boucher and Reddy (2008) (black), and the three distributions obtained from the inter-comparison exercise data, i.e., CMIP3 (red), CMIP3* (blue) and CMIP5 (green). One can notice that the CMIP5 IRF is highest for the first 4–5 yr, but lowest in the 100–1000 yr range, where it additionally shows a considerable larger spread. For the period 100–1000 yr, one can further observe a considerable difference between CMIP3 and CMIP3*, and some agreement between CMIP3* and BR08.

ESDD
3, 935–977, 2012

The top right panel in Fig. 2 shows the integrated temperature IRF presented in Eq. (6). The CMIP3 and CMIP3* approach are rather similar below 100 yr, but deviate strongly later. The CMIP5 curve is considerably higher the first 10 yr due to its smaller fast response time, and lies between the CMIP3 and CMIP3* curves for the period after 100 yr. The asymptotic value of these integrated temperature IRF curves for $t \rightarrow \infty$ gives the total climate sensitivity, which is clearly highest for BR07 and CMIP3*. The climate sensitivity shows similar spreads among the IRFs, i.e., 0.3 K for CMIP3, 0.4 K for CMIP5 and 0.5 K for CMIP3* (10–90 % spread).

The best estimates for the temperature IRF parameters when calibrated to the individual AOGCMs are shown as the separate symbols in the bottom panel. Again, the derived distributions are represented by the ellipses (the area within the ellipses represents 80 % of the distribution). The temperature IRF contains two modes, where the fast mode has a response time in the order of 2–10 yr, and the slow mode in the order of 30–500 yr. The CMIP3* approach gives for (τ_1, f_1) results similar to CMIP3, but for (τ_2, f_2) considerably higher values, reflecting a considerably higher total climate sensitivity. The CMIP5 results show relatively small values for τ_1 which is probably related to the type of experiment, i.e., an instantaneous increase in the radiative forcing (Olivié et al., 2012). The CMIP5 results also show lower values for the time constant of the slow mode τ_2, together with a relatively large spread – this is probably related to the short length of the CMIP5 experiments

The values of $\bar{\boldsymbol{x}}$ and $\boldsymbol{\Sigma}$ describing the different derived CO_2 and temperature IRF distributions can be found in Tables 5 and 6.

4.2 Impact of spread in CO_2 IRF on metrics

Based on the CO_2 IRF and temperature IRF distributions presented above, we calculated GWP, GTP and iGTP metric values including their spread, for different species and different time horizons. To take into account the spread in the IRFs, we perform Monte-Carlo simulations.

ESDD
3, 935–977, 2012

Figure 3 shows the estimates of GWP, GTP, and iGTP for time horizons of 20, 50, and 100 yr for BC, CH_4, N_2O, and SF_6. Note that all parameter values such as specific radiative forcings, life times of non-CO_2-species, and coefficients of the reference IRFs J07 and BR08 are taken just like in IPCC (2007). We use four different CO_2 IRFs to calculate metric values, i.e., J07 (black, top row), C^4MIP(u) (red, second row), C^4MIP(c) (blue, third row), and LTMIP (green, last row). For every species and time horizon is indicated in the top row the J07 result – the exact value is explicitly mentioned right of it. The results from the three IRF distributions are given on the three following lines, indicating the 10-, 25-, 50- (indicated in black), 75-, and 90-percentile values. The number added on the right hand side of this bar gives the ratio between the median value of the distribution and the reference value from J07. The bars at the right illustrate the spread within the distribution by indicating how much the 10-, 25-, 75-, and 90-percentile values differ (in %) from the median value of the distribution. The numbers (in %) at left and right indicate how much the 10- and 90-percentile values deviate from the median value.

For GWP, shown in the top panels of Fig. 3, the median values from C^4MIP(u) and C^4MIP(c) are significantly higher than the J07 values for time horizons smaller than 100 yr (e.g., 43 % larger for H = 20 yr), and smaller for larger time horizons (not shown). This is caused by the fact that the C^4MIP(u) IRF and C^4MIP(c) IRF are initially lower than the J07 IRF, but higher for later times. The LTMIP IRF gives in general lower values than J07 (varying between 22 % lower for H = 20 yr to 32 % lower for H = 100 yr), but the evolution of the values as a function of the time horizon is rather similar to J07. This is coherent with the observation that the LTMIP IRF is consistently below the J07 IRF. As the CO_2 IRF only affects the denominator (i.e., $AGWP_{CO_2}$) in the expression for GWP, this impact is identical for the four species we study here, giving identical ratios in Fig. 3.

GTP and iGTP values are influenced both by the CO_2 IRF and the temperature IRF. To facilitate the interpretation of the results, we look here first only to the impact of the spread in the CO_2 IRFs. The middle and lower panels in Fig. 3 show therefore GTP

ESDD
3, 935–977, 2012

and iGTP values, respectively, and their spread for different time horizons based on different CO_2 IRF distributions, but using always the BR08 temperature IRF. For H = 20 yr, C^4MIP(u) and C^4MIP(c) give higher GTP values than J07, and LTMIP lower value than J07 (as for GWP). The J07 IRF gives higher values now already from a time horizon of 100 yr for all species. Again, the behaviour as a function of the time horizon is rather similar between LTMIP and J07, but considerably different for C^4MIP(u) and C^4MIP(c). For example for SF_6, one finds almost constant values for the GTP as a function of the time horizon for C^4MIP(u) and C^4MIP(c), but increasing values as a function of the time horizon value for LTMIP and J07. One can also see that the variation of the metrics as a function of the time horizon or choice of CO_2 IRF is very similar for the three metrics. The closest agreement can be seen between GWP and iGTP (Peters et al., 2011).

A better impression of the spread in the metric values resulting from the width of the CO_2 IRF distributions is given by the relative spreads in Fig. 3 for the GWP, GTP, and iGTP metric. These spreads are identical for all species, and do not vary much among the different metrics, with values between −7 % and 32 %. The LTMIP CO_2 IRF induces more asymmetric uncertainty intervals than C^4MIP(u) and C^4MIP(c), which is most pronounced for the H = 20 yr time horizon. This asymmetry is a consequence of the asymmetric uncertainty distribution in the LTMIP CO_2 IRF, as can be seen in the left panel of Fig. 1.

Finally, we mention that for BC and CH_4 the metric values decay strongly as a function of the time horizon, that for N_2O they are rather insensitive to the time horizon, and that for SF_6 metric values increase as a function of the time horizon.

4.3 Impact of spread in temperature IRF on metrics

For the GTP and iGTP metric, there is also a dependency on the temperature IRF. Here we investigate this dependency by using different temperature IRFs and their spread, but using always the reference J07 CO_2 IRF. One must be aware that now in GTP and iGTP both the numerator and denominator are influenced (see Eqs. 9 to 12).

ESDD
3, 935–977, 2012

The upper panels in Fig. 4 show GTP values and their spread for different time horizons based on different temperature IRFs. One observation is the strong difference between the behaviour of BC and CH_4 compared with N_2O and SF_6. N_2O and SF_6 show very small differences for the different temperature IRFs, while BC shows ratios of the median value varying in the range 0.50–1.86, and for CH_4 in the range 0.81–1.36. We see, e.g., that for BC and CH_4 using the CMIP3, CMIP3*, or CMIP5 IRF underestimates the metric values with respect to BR08 for the smallest time horizon (H = 20 yr), but overestimates it for (H = 50 yr) and this is most pronounced for the CMIP5 IRF. This behaviour can be explained by the fact that GTP is the ratio of the AGTP of a certain species divided by the AGTP of CO_2. As BC has a very short life time, the time dependence of its AGTP is very similar to the temperature IRF curve in the top left panel of Fig. 2 (as BC is only very short in the atmosphere, the RF it creates is also very short in time and is comparable to a δ-pulse, and its temperature response proportional to IRF_T). On the other hand, because CO_2 has characteristics of a longer life time, the time dependence of its AGTP will be more similar to the integrated temperature IRF curve in the top right panel of Fig. 2 (to zero-th order, a pulse emission of CO_2 stays permanently in the atmosphere, causing a step increase in the RF and therefore a temperature response comparable to the integrated temperature IRF). For H = 20 yr, we see that the CMIP5 IRF is much lower than BR08 (determining the numerator), while the integrated CMIP5 IRF is similar to BR08 (determining the denominator). This explains why the value for BC at H=20 yr is so low using the CMIP5 IRF. The inverse behaviour for H=50 yr is caused by the fact that now the denominator is slightly higher for the temperature IRF (see top left panel in Fig. 2), while the denominator is consistently smaller. The changing relative positions of the IRF curves is clearly reflected in the GTP metric values. To a lesser extend the same reasoning is true for CH_4, as it still has a relative short life time with respect to CO_2.

The general good correspondence for N_2O and SF_6 with BR08 for all three time horizons is caused by the fact that the AGTP of N_2O and SF_6 as a function of time behaves very much as the integrated temperature IRF, as CO_2 does to some extend

ESDD
3, 935–977, 2012

(see above). This leads to the fact that variations in the numerator and denominator of the GTP expression will be very similar and cancel out for N_2O and SF_6.

The right bars in Fig. 4 show the relative spread in GTP values due to the spread in the temperature IRFs. The amount of spread is strongly dependant on the species and the time horizon. BC shows uncertainties around 40–60 % for all time horizons up to H = 100 yr. This spread increases drastically when using the CMIP5 IRF for larger time horizons (not shown). For CH_4, the spread is smaller than for BC when looking at time horizons of 20 and 50 yr, but rather similar for larger time horizons. For N_2O, very small ranges are found up to time horizons of 100 yr, but increasing after that (not shown). For SF_6 we find small uncertainty ranges for all time horizons.

The iGTP values are shown in the bottom panels of Fig. 4. One finds much lower deviations and much smaller spreads, since the iGTP is an integrated version of the GTP. The strongest deviation from 1 for the ratio for BC is now 0.85, and the relative spread is between −7 % and +8 %. The reduced deviation, e.g. for BC, can be explained by the fact that the numerator in iAGTP is now the integral of the curve show in the top left panel of Fig. 4. As the CMIP5 curve up to 20 yr lies partially above and partially below the BR08 curve, the integrals are not that different H = 20 yr (0.85). For H = 50 yr and H = 100 yr this difference is even further reduced (0.96 and 1.00). Accordingly, also the spread is strongly reduced.

4.4 Simultaneous impact of spread in CO_2 and temperature IRFs on metrics

Whereas we have presented above for GTP and iGTP the impact induced by spread in CO_2 and temperature IRFs separately, we show here their combined impact on the metric values. The reference case is now the combination of the J07 CO_2 IRF and the BR08 temperature IRF. Using the derived three CO_2 IRF and three temperature IRF distributions, one can make 9 combinations. Figure 5 shows the GTP and iGTP values when using the reference IRFs and when using the 9 possible combinations of the derived IRF distributions. We acknowledge that combining CO_2 and temperature IRFs in such a manor might lead to inconsistent parameter combinations, but we note that

ESDD
3, 935–977, 2012

this problem is ignored in the metric literature which routinely combines J07 and BR08 for GTP values.

For GTP, one observes ratios that vary in the range 0.37–1.66 for BC, 0.61–1.33 for CH_4, 0.66–1.37 for N_2O, and 0.66–1.39 for SF_6. These ratios are a result of the ratios in Figs. 3 and 4, and can actually be very well approximated by their product. For example, the value of 0.37 for BC at H=20 yr (LTMIP–CMIP5), is very close to $0.76 \times 0.50 = 0.38$, or the value of 0.76 for CH_4 at H=100 yr (LTMIP–CMIP3) is close to $0.66 \times 1.13 = 0.75$.

For iGTP, we see ratios in the range 0.68–1.45 for BC, 0.70–1.47 for CH4, 0.70–1.48 for N_2O, and 0.70–1.49 for SF_6. Again one can check that for the chosen combination of IRFs, the deviation is close to the product of ratios in Figs. 3 and 4. These combined ratios represent mainly the impact from the CO_2 IRF as the the ratios in Fig.4 are all close to 1 for iGTP.

The spread in GTP resulting from the width of IRF distributions is large for BC, slightly smaller for CH_4 at small time horizons, and rather small for N_2O and SF_6. The spread is a combination of the separate spreads in Figs. 3 and 4 – it is larger than the individual spreads, and mainly determined by its largest contributor. The spread in GTP for BC is mainly determined by the temperature IRF, for CH_4 it is determined by the CO_2 IRF for short time horizons (H = 20 yr) and by the temperature IRF for large time horizons (H = 100 yr). For N_2O and SF_6 it is determined by the spread in the CO_2 IRF. Finally, for iGTP the spread is mainly determined by the spread caused by the CO_2 IRF.

5 Conclusions

The aim of this study was twofold. The first aim was deriving CO_2 and temperature IRF distributions based on the behaviour of different CC-models and AOGCMs. The second aim was analyzing how the spread in these IRFs influences emission metrics.

The estimate of IRF distributions has been based on simulations from four different model inter-comparison projects, i.e., C^4MIP and LTMIP for estimating CO_2 IRF

ESDD
3, 935–977, 2012

distributions, and CMIP3 and CMIP5 for estimating temperature IRF distributions. C^4MIP contained both experiments with and without taking into account the climate impact on the atmospheric CO_2 mixing ratio, resulting in two different CO_2 IRF distributions. From CMIP3, we also derived an additional temperature IRF where climate sensitivity estimates from a separate MLO-AGCM experiment were used. As reference for comparison we used the CO_2 IRF from IPCC (2007) (in the text noted as J07) and the temperature IRF from Boucher and Reddy (2008) (in the text noted as BR08).

The behaviour of the three derived CO_2 IRFs is rather different from the reference IRF in J07. The C^4MIP IRFs decrease strongly the first year, after which they remain rather flat. The LTMIP IRF has a tendency to remain considerably higher than J07, and giving similar values to J07 only after 1000 yr. These differences probably arise from different experimental setups. The width of the C^4MIP IRF distribution increases strongly the first year, but than remains rather constant for longer time scales. For LTMIP, the width increase as a function of time is smaller, and the width of the distribution decreases again for long time scales (100–1000 yr). In general, the order of magnitude of the width of the IRF distributions is similar for all three CO_2 IRF distributions.

Concerning temperature IRF, the three distributions coincide in general rather well, but also show specific differences. Whereas the CMIP3 results coincide with BR08 for the first 10 yr and CMIP5 is considerably higher than BR08 for the same period, all three derived distributions are very similar in the period 20–100 yr but below the BR08 value. For long time scales, they all give considerably lower values than BR08. The width of all IRF distributions is in general rather similar, becoming larger for longer time scales. For the temperature IRF we mention the rather similar spread in climate sensitivity, i.e., 0.3 K for CMIP3, 0.4 K for CMIP5 and 0.5 K for CMIP3* (10–90 % spread). A noticeable difference exists in the behaviour of the CMIP5 IRF, which shows a rather large relative spread for times larger than 200 yr. Although for large time the BR08 IRF is considerably higher than the new IRFs, BR08 falls still within the high end of CMIP3* distribution.

ESDD
3, 935–977, 2012

The spread in IRFs has a considerable impact on the value of the GWP, GTP and iGTP metrics. The impact from spread in the CO_2 IRF has a very similar impact on all three emission metrics. The impacts are also equal for all studied species (BC, CH_4, N_2O, and SF_6). The main characteristics of the CO_2 IRFs have a straightforward impact on the emission metrics: the higher LTMIP CO_2 IRF gives lower metric values. The fact that the C^4MIP IRF is initially lower, but higher for later times is reflected in higher metric values for short time horizons, turning finally in smaller values for longer time horizons. The spread within all the IRF distributions creates very similar spreads, varying between −7 % and +32 %.

The GTP and iGTP metrics are also influenced by the spread in the temperature IRFs. For GTP, the temperature IRF induced spread is significantly larger than the CO_2 induced spread for short lived species as BC for all studied time horizons, and for CH_4 for the larger time horizons. Using the CMIP5 temperature IRF, spreads are considerably larger than using the CMIP3 or CMIP3* ones. On the other hand, one sees that for N_2O and SF_6 very few differences are found among the GTP values, although the temperature IRFs differs considerably. This is caused by the appearance of the temperature IRF both in the numerator and denominator of the GTP expressions, and the relative long lifetimes of CO_2, N_2O and SF_6.

Finally, due to the integrative character of iGTP, the temperature IRF induced spread is much smaller than for GTP. The temperature IRF induced spread is even smaller than the CO_2 induced spread.

Part of the differences between the derived IRFs can be attributed to the type of experiment performed with the CC-models and AOGCMs. Pulse-type experiments as in LTMIP are very useful to quantify CO_2 IRFs, but the LTMIP IRF is probably high biased due to the high emission amount. The gradual evolution of the CO_2 emission scenario in C^4MIP makes it difficult to uniquely determine the CO_2 IRF. Therefore we think it would be very useful to do LTMIP-like scenarios but with smaller pulse sizes. The CMIP5 experiment with its abrupt forcing change is in principal very useful to derive temperature IRFs. However, these experiments also show in general a lower value

ESDD
3, 935–977, 2012

for the slow time scale due to the short length of the simulation. Extending these scenario up to ~500 yr would allow to better constrain the parameters in the temperature IRF, and especially allow to use the IRFs for larger times. Finally, a range of several different idealized experiments with different sizes of the amplitudes would allow for an estimation of the non-linearities in the system. This has partially been done in Eby et al. (2009), however, they explored mainly the range of very large emission pulses.

The use of the presented metric distributions should be taken with care. They represent only estimates of the spreads related to the behaviour of the underlying CC-model or AOGCM, and the model spread may not be indicative of the true uncertainties. The estimates do not take into account other reasons for spread that might impact metric values, such as uncertainties on the life time of BC, CH_4, N_2O or SF_6. One should also be aware that the analysis here provides uncertainties when comparing arbitrary species with CO_2, but does not provide uncertainties for the comparison of two non-CO_2 species nor absolute metric values for single species. This has not been discussed, but this analysis can be performed based on the IRF distributions presented in this work. Similarly, impacts on emission metric for time horizons larger than 100 yr can easily be studied.

Acknowledgements. We thank the different modelling groups participating in the CMIP3, C^4MIP, LTMIP and CMIP5 model inter-comparison projects for producing and making available their model output. We thank M. Eby and D. Archer for providing the LTMIP data, and P. Friedlingstein for providing the C^4MIP data. We acknowledge the World Climate Research Programme's Working Group on Coupled Modelling, which is responsible for CMIP. For CMIP the U.S. Department of Energy's Program for Climate Model Diagnosis and Inter-comparison provides coordinating support and led development of software infrastructure in partnership with the Global Organization for Earth System Science Portals.

ESDD
3, 935–977, 2012

References

Archer, D., Eby, M., Brovkin, V., Ridgwell, A., Cao, L., Mikolajewicz, U., Caldeira, K., Matsumoto, K., Munhoven, G., Montenegro, A., and Tokos, K.: Atmospheric lifetime of fossil fuel carbon dioxide, Annu. Rev. Earth Planet. Sci., 37, 117–134, doi:10.1146/annurev.earth.031208.100206, 2009. 937, 941, 946, 947, 968

Boucher, O. and Reddy, M. S.: Climate trade-off between black carbon and carbon dioxide emissions, Energ. Policy, 36, 193–200, doi:10.1016/j.enpol.2007.08.039, 2008. 939, 940, 943, 945, 947, 953, 960, 968, 970

Caldeira, K. and Kasting, J. F.: Insensitivity of global warming potentials to carbon dioxide emission scenarios, Nature, 366, 251–253, 1993. 938

Cao, L., Eby, M., Ridgwell, A., Caldeira, K., Archer, D., Ishida, A., Joos, F., Matsumoto, K., Mikolajewicz, U., Mouchet, A., Orr, J. C., Plattner, G.-K., Schlitzer, R., Tokos, K., Totterdell, I., Tschumi, T., Yamanaka, Y., and Yool, A.: The role of ocean transport in the uptake of anthropogenic CO_2, Biogeosciences, 6, 375–390, doi:10.5194/bg-6-375-2009, 2009. 947

Collins, W. J., Sitch, S., and Boucher, O.: How vegetation impacts affect climate metrics for ozone precursors, J. Geophys. Res., 115, D23308, doi:10.1029/2010JD014187, 2010. 938

Cox, P. M., Betts, R. A., Jones, C. D., Spall, S. A., and Totterdell, I. J.: Acceleration of global warming due to carbon cycle feedbacks in acoupled climate model, Nature, 408, 184–187, 2000. 946

Danabasoglu, G. and Gent, P. R.: Equilibrium climate sensitivity: Is it accurate to use a slab ocean model?, J. Climate, 22, 2494–2499, doi:10.1175/2008JCLI2596.1, 2009. 939

Dufresne, J.-L., Friedlingstein, P., Berthelot, M., Bopp, L., Ciais, P., Fairhead, L., Treut, H. L., and Monfray, P.: On the magnitude of positive feedback between future climate change and the carbon cycle, Geophys. Res. Lett., 29, 1405, doi:10.1029/2001GL013777, 2002. 946

Eby, M., Zickfeld, K., Montenegro, A., Archer, D., Meissner, K. J., and Weaver, A. J.: Lifetime of anthropogenic climate change: millennial time scales of potential CO_2 and surface temperature perturbations, J. Climate, 22, 2501–2511, doi:10.1175/2008JCLI2554.1, 2009. 938, 947, 962

Friedlingstein, P., Dufresne, J.-L., Cox, P. M., and Rayner, P.: How positive is the feedback between climate change and the carbon cycle?, Tellus, 55B, 692–700, doi:10.1034/j.1600-0889.2003.01461.x, 2003. 946

ESDD
3, 935–977, 2012

Friedlingstein, P., Cox, P., Betts, R., Bopp, L., von Bloh, W., Brovkin, V., Cadule, P., Doney, S., Eby, M., Fung, I., Bala, G., John, J., Jones, C., Joos, F., Kato, T., Kawamiya, M., Knorr, W., Lindsay, K., Matthews, H. D., Raddatz, T., Rayner, P., Reick, C., Roeckner, E., Schnitzler, K.-G., Schnur, R., Strassmann, K., Weaver, A. J., Yoshikawa, C., and Zeng, N.: Climate-carbon cycle feedback analysis: results from the C^4MIP model intercomparaison, J. Climate, 19, 3337–3353, 2006. 938, 946

Fuglestvedt, J. S., Berntsen, T. K., Godal, O., Sausen, R., Shine, K. P., and Skodvin, T.: Metrics of climate change: Assessing radiative forcing and emission indices, Climatic Change, 58, 267–331, doi:10.1023/A:1023905326842, 2003. 937

Fuglestvedt, J. S., Shine, K. P., Berntsen, T., Cook, J., Lee, D. S., Stenke, A., Skeie, R. B., Velders, G. J. M., and Waitz, I. A.: Transport impacts on atmosphere and climate: Metrics, Atmos. Environ., 44, 4648–4677, doi:10.1016/j.atmosenv.2009.04.044, 2010. 937, 967

Gillett, N. P. and Matthews, H. D.: Accounting for carbon cycle feedbacks in a comparison of the global warming effects of greenhouse gases, Environ. Res. Lett., 5, 034011, doi:10.1088/1748-9326/5/3/034011, 2010. 938, 939

Gloor, M., Sarmiento, J. L., and Gruber, N.: What can be learned about carbon cycle climate feedbacks from the CO_2 airborne fraction?, Atmos. Chem. Phys., 10, 7739–7751, doi:10.5194/acp-10-7739-2010, 2010. 953

Hasselmann, K., Sausen, R., Maier-Reimer, E., and Voss, R.: On the cold start problem in transient simulations with coupled atmosphere-ocean models, Clim. Dynam., 9, 53–61, 1993. 939, 943

Held, I. M., Winton, M., Takahashi, K., Delworth, T., Zeng, F., and Vallis, G. K.: Probing the fast and slow components of global warming by returning abruptly to preindustrial forcing, J. Climate, 23, 2418–2527, doi:10.1175/2009JCLI3466.1, 2010. 939

Hooss, K. G.: Aggregate models of climate change: development and applications, Ph.D. thesis, University of Hamburg, Hamburg, Germany, 2001. 938

Houghton, J. T., Jenkins, G. J., and Ephraums, J. J., eds.: Climate change: the IPCC scientific assessment, Cambridge University Press, Cambridge, United Kingdom and New York, NY, USA, 1990. 937

IPCC: Climate change 2001: the scientific basis. Contribution of working group I to the third assessment report of the intergovernmental panel on climate change, Cambridge University Press, Cambridge, United Kingdom and New York, NY, USA, 881 pp., 2001. 938, 942

ESDD
3, 935–977, 2012

IPCC: Climate change 2007: the physical science basis. Contribution of working group I to the fourth assessment report of the intergovernmental panel on climate change, Cambridge University Press, Cambridge, United Kingdom and New York, NY, USA, 996 pp., 2007. 938, 940, 942, 945, 947, 948, 955, 960, 967, 968, 969

Joos, F., Bruno, M., Fink, R., Siegenthaler, U., Stocker, T. F., Quéré, C. L., and Sarmiento, J.: An efficient and accurate representation of complex oceanic and biospheric models of anthropogenic carbon uptake, Tellus, 48B, 397–417, doi:10.1034/j.1600-0889.1996.t01-2-00006, 1996. 938

Joos, F., Prentice, I. C., Sitch, S., Meyer, R., Hooss, G., Plattner, G.-K., Gerber, S., and Hasselmann, K.: Global warming feedbacks on terrestrial carbon uptake under the Intergovernmental Panel on Climate Change (IPCC) Emission Scenarios, Global Biogeochem. Cy., 15, 891–907, doi:10.1029/2000GB001375, 2001. 940, 945

Li, S. and Jarvis, A.: Long run surface temperature dynamics of an A-OGCM: the HadCM3 4xCO_2 forcing experiment revisited, Clim. Dynam., 33, 817–825, doi:10.1007/s00382-009-0581-0, 2009. 939, 943, 947

Manabe, S. and Stouffer, R. J.: Multiple-century response of a couple ocean-atmosphere model to an increase of atmospheric carbon dioxide, J. Climate, 7, 5–23, 1994. 939

Nakicenovic, N., Alcamo, J., Davis, G., de Vries, B., Fenhann, J., Gaffin, S., Gregory, K., Grübler, A., Jung, T. Y., Kram, T., Rovere, E. L. L., Michaelis, L., Mori, S., Morita, T., Pepper, W., Pitcher, H., Price, L., Riahi, K., Roehrl, A., Rogner, H.-H., Sankovski, A., Schlesinger, M., Shukla, P., Smith, S., Swart, R., van Rooijen, S., Victor, N., and Dadi, Z.: Emissions scenarios, Cambridge University Press, Cambridge, United Kingdom and New York, NY, USA, 2000. 946

Olivié, D. and Stuber, N.: Emulating AOGCM results using simple climate models, Clim. Dynam., 35, 1257–1287, doi:10.1007/s00382-009-0725-2, 2010. 939, 949, 950

Olivié, D. J. L., Peters, G. P., and Sain-Martin, D.: Atmospheric response time scales estimated from AOGCM experiments, J. Climate, accepted, 2012. 939, 949, 954

Peters, G. P., Aamaas, B., Berntsen, T., and Fuglestvedt, J. S.: The integrated global temperature change potential (iGTP) and relationships between emission metrics, Environ. Res. Lett., 6, 044021, doi:10.1088/1748-9326/6/4/044021, 2011. 937, 956

Reisinger, A., Meinshausen, M., Manning, M., and Bodeker, G.: Uncertainties of global warming metrics: CO_2 and CH_4, Geophys. Res. Lett., 37, L14707, doi:10.1029/2010GL043803, 2010. 940

ESDD
3, 935–977, 2012

Sausen, R. and Schumann, U.: Estimates of the climate response to aircraft CO_2 and NO_x emissions scenarios, Climate change, 44, 27–58, 2000. 939

Shine, K. P., Fuglestvedt, J., Hailemariam, K., and Stuber, N.: Alternatives to the global warming potential for comparing climate impacts of emissions of greenhouse gases, Climatic Change, 68, 281–302, doi:10.1007/s10584-005-1146-9, 2005. 937, 939

Shine, K. P., Berntsen, T. K., Fuglestvedt, J. S., Skeie, R. B., and Stuber, N.: Comparing the climate effect of emissions of short- and long-lived climate agents, Phil. Trans. R. Soc. A, 365, 1903–1914, doi:10.1098/rsta.2007.2050, 2007. 937

Sitch, S., Cox, P. M., Collins, W. J., and Huntingford, C.: Indirect radiative forcing of climate change through ozone effects on the land-carbon sink, Nature, 448, 791–794, doi:10.1038/nature06059, 2007. 938

Stouffer, R.: Time scales of climate response, J. Climate, 17, 209–217, 2004. 939

Tarantola, A.: Inverse problem theory and methods for model parameter estimation, Society for Industrial and Applied Mathematics, Philadelphia, 342 pp., 2005. 949

Taylor, K. E., Stouffer, R. J., and Meehl, G. A.: An overview of CMIP5 and the experiment design, B. Am. Meteorol. Soc., 93, 485–498, doi:10.1175/BAMS-D-11-00094.1, 2012. 948, 968

Yang, H. and Zhu, J.: Equilibrium thermal response timescale of global oceans, Geophys. Res. Lett., 38, L14711, doi:10.1029/2011GL048076, 2011. 939

ESDD
3, 935–977, 2012

Table 1. Life time and specific radiative forcing of BC, CH_4, CO_2, N_2O, and SF_6 (see IPCC, 2007 and Fuglestvedt et al., 2010).

		BC	CH_4	CO_2	N_2O	SF_6
τ	[yr]	0.02	12	–	114	3200
A_X	[$W\,m^{-2}\,kg^{-1}$]	1.96×10^{-9}	1.82×10^{-13}	1.81×10^{-15}	3.88×10^{-13}	2.00×10^{-11}

ESDD
3, 935–977, 2012

Table 2. Overview of the different data sets used to derive CO_2 and temperature IRFs. The number of models used here might be lower than the number of models participating in the inter-comparison project.

	Experimental setup	Length [yr]	Models [#]	Release	Reference
J07	Pulse CO_2 emission	1000	1	2007	IPCC (2007)
C^4MIP	Gradual CO_2 emission (SRES A2)	240	11	2006	IPCC (2007)
LTMIP	Pulse CO_2 emission	10 000	9	2009	Archer et al. (2009)
BR08	Linear RF increase + stabilization	1000	1	2008	Boucher and Reddy (2008)
CMIP3	Linear RF increase + stabilization	70–300	15	2006	IPCC (2007)
CMIP5	Step RF increase/linear RF increase	140–150	15	2011	Taylor et al. (2012)

ESDD
3, 935–977, 2012

Table 3. Value of the parameters in the CO_2 IRFs: J07 is the IRF used in IPCC (2007), and C^4MIP(u), C^4MIP(c) and LTMIP are the IRFs derived using C^4MIP and LTMIP data. In all IRFs is $\tau_0 = \infty$. C^4MIP(c) represents an experiment with a temperature feedback and C^4MIP(u) without a temperature feedback. The median, and 10- and 90-percentile values are indicated.

	τ_1 [yr]	τ_2 [yr]	τ_3 [yr]	a_0	a_1	a_2	a_3
J07	172.9	18.51	1.19	0.217	0.259	0.338	0.186
C^4MIP(u)	1213.22 ± 65 %	2.61 ± 66 %	0.31 ± 85 %	0.33 ± 20 %	0.12 ± 50 %	0.09 ± 41 %	0.46 ± 24 %
C^4MIP(c)	1796.74 ± 49 %	1.80 ± 58 %	0.24 ± 64 %	0.41 ± 25 %	0.11 ± 49 %	0.08 ± 26 %	0.40 ± 28 %
LTMIP	270.59 ± 38 %	33.70 ± 111 %	1.65 ± 36 %	0.20 ± 11 %	0.50 ± 26 %	0.22 ± 36 %	0.08 ± 153 %

ESDD
3, 935–977, 2012

Table 4. Value of the parameters in the temperature IRFs: BR08 is the IRF used in Boucher and Reddy (2008), and CMIP3, CMIP3* and CMIP5 are the IRFs derived using CMIP3 and CMIP5 data. The CMIP3 IRF is based on AOGCM experiments alone, while the CMIP3* IRF additionally includes the independently estimated climate sensitivities. The median, and 10- and 90-percentile values are indicated.

	τ_1 [yr]	τ_2 [yr]	f_1 [K W^{-1} m^2]	f_2 [K W^{-1} m^2]
BR08	8.4	409.5	0.631	0.429
CMIP3	7.15 ± 35 %	105.55 ± 38 %	0.48 ± 30 %	0.20 ± 52 %
CMIP3*	7.24 ± 43 %	244.44 ± 130 %	0.49 ± 25 %	0.36 ± 91 %
CMIP5	2.57 ± 46 %	82.24 ± 192 %	0.43 ± 29 %	0.32 ± 59 %

ESDD
3, 935–977, 2012

Table 5. Value of mean vector $\bar{x}$ and covariance matrix $\mathbf{\Sigma}$ in the CO_2 IRF distributions (see Eq. 16) derived using C^4MIP and LTMIP data. The distribution is for the logarithm of the IRF parameters.

	$\log\tau_1$	$\log\tau_2$	$\log\tau_3$	$\log b_1$	$\log b_2$	$\log b_3$
			C^4MIP(u)			
			$\bar{x}$			
	7.101	0.959	−1.161	−1.047	−1.270	0.313
			$\mathbf{\Sigma}$			
$\log\tau_1$	0.153	−0.153	−0.178	−0.133	−0.153	−0.034
$\log\tau_2$	−0.153	0.160	0.190	0.147	0.156	0.018
$\log\tau_3$	−0.178	0.190	0.231	0.183	0.183	0.007
$\log b_1$	−0.133	0.147	0.183	0.153	0.137	−0.011
$\log b_2$	−0.153	0.156	0.183	0.137	0.154	0.028
$\log b_3$	−0.034	0.018	0.007	−0.011	0.028	0.056
			C^4MIP(c)			
	$\log\tau_1$	$\log\tau_2$	$\log\tau_3$	$\log b_1$	$\log b_2$	$\log b_3$
			$\bar{x}$			
	7.494	0.590	−1.435	−1.348	−1.620	−0.032
			$\mathbf{\Sigma}$			
$\log\tau_1$	0.098	−0.106	−0.097	−0.101	−0.104	−0.090
$\log\tau_2$	−0.106	0.130	0.132	0.139	0.122	0.079
$\log\tau_3$	−0.097	0.132	0.150	0.158	0.120	0.047
$\log b_1$	−0.101	0.139	0.158	0.171	0.125	0.049
$\log b_2$	−0.104	0.122	0.120	0.125	0.116	0.083
$\log b_3$	−0.090	0.079	0.047	0.049	0.083	0.118
			LTMIP			
	$\log\tau_1$	$\log\tau_2$	$\log\tau_3$	$\log b_1$	$\log b_2$	$\log b_3$
			$\bar{x}$			
	5.601	3.517	0.501	0.933	0.139	−0.959
			$\mathbf{\Sigma}$			
$\log\tau_1$	0.065	0.030	−0.019	−0.006	−0.014	−0.011
$\log\tau_2$	0.030	0.342	0.054	0.094	−0.106	−0.389
$\log\tau_3$	−0.019	0.054	0.060	0.043	−0.022	−0.102
$\log b_1$	−0.006	0.094	0.043	0.064	−0.038	−0.131
$\log b_2$	−0.014	−0.106	−0.022	−0.038	0.039	0.127
$\log b_3$	−0.011	−0.389	−0.102	−0.131	0.127	0.481

ESDD
3, 935–977, 2012

Table 6. Value of mean vector $\bar{x}$ and covariance matrix $\mathbf{\Sigma}$ in the temperature IRF distributions (see Eq. 16) derived using CMIP3 and CMIP5 data.

	CMIP3			
	$\log \tau_1$	$\log \tau_2$	$\log f_1$	$\log f_2$
		$\bar{x}$		
	1.967	4.659	−0.739	−1.612
		$\mathbf{\Sigma}$		
$\log \tau_1$	0.056	−0.033	0.012	0.012
$\log \tau_2$	−0.033	0.064	−0.005	0.028
$\log f_1$	0.012	−0.005	0.042	−0.000
$\log f_2$	0.012	0.028	−0.000	0.110

	CMIP3*				CMIP5				
	$\log \tau_1$	$\log \tau_2$	$\log f_1$	$\log f_2$		$\log \tau_1$	$\log \tau_2$	$\log f_1$	$\log f_2$
		$\bar{x}$					$\bar{x}$		
	1.980	5.499	−0.714	−1.031		0.945	4.410	−0.842	−1.154
		$\mathbf{\Sigma}$					$\mathbf{\Sigma}$		
$\log \tau_1$	0.080	−0.100	0.011	−0.066	$\log \tau_1$	0.089	0.147	0.038	0.034
$\log \tau_2$	−0.100	0.423	−0.005	0.102	$\log \tau_2$	0.147	0.701	0.019	0.001
$\log f_1$	0.011	−0.005	0.031	0.011	$\log f_1$	0.038	0.019	0.040	0.024
$\log f_2$	−0.066	0.102	0.011	0.259	$\log f_2$	0.034	0.001	0.024	0.133

ESDD
3, 935–977, 2012

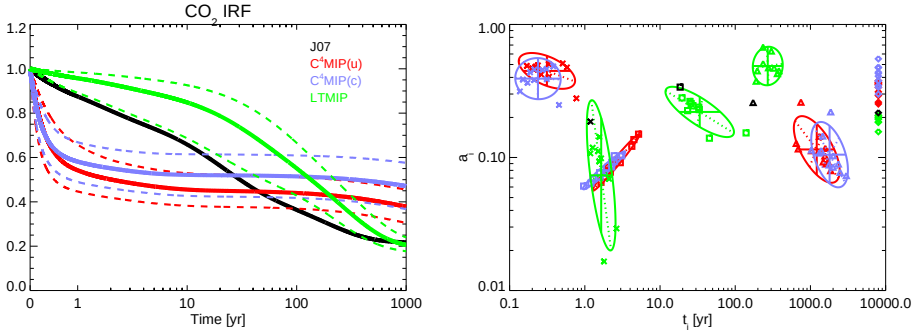

Fig. 1. Overview of four different CO_2 IRF distributions: J07 (black), C^4MIP(u) (red), C^4MIP(c) (blue), and LTMIP (green). Left: IRF as in Eq. (1) with median (full line) and 10- and 90-percentile values (dashed lines) indicated. The horizontal axis is linear from 0 to 1 yr, and logarithmic from 1 to 1000 yr. Right: estimates for the parameters in the CO_2 IRFs, where every single dot corresponds with one of the four modes, i.e. (τ_0, a_0) (diamond), (τ_1, a_1) (triangle), (τ_2, a_2) (square), or (τ_3, a_3) (cross). The (τ_0, a_0) tuples (which would fall off the figure as $\tau_0 = \infty$) are given at the right of the figure. The individual dots represent the best estimates for the individual CC-models, while the ellipses represent the distributions derived from the individual estimates, grouped per inter-comparison project. Inside the ellipses falls 80 % of the distribution.

ESDD
3, 935–977, 2012

The impact of model variation on emission metrics

D. J. L. Olivié and G. P. Peters

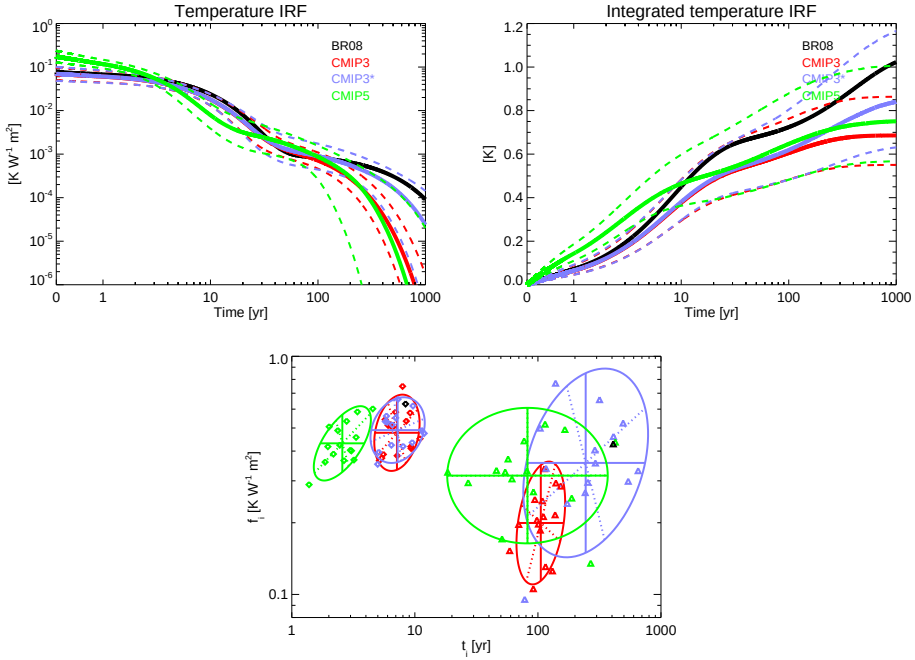

Fig. 2. Overview of four different temperature IRF distributions: BR08 (black), CMIP3 (red), CMIP3* (blue), and CMIP5 (green). Top left: IRF as in Eq. (5) with median (full line) and 10- and 90-percentile values (dashed lines) indicated. Note the logarithmic scale on the vertical axis, and that the horizontal axis is linear from 0 to 1 yr, and logarithmic from 1 to 1000 yr. Top right: integrated temperature IRFs as in Eq. (6). Bottom: estimates of the parameters in the temperature IRF. Every single dot corresponds with one of the two modes in one AOGCM, i.e., the fast mode (τ_1, f_1) (diamonds) or the slow mode (τ_2, f_2) (triangles). The ellipses represent the distributions of the IRF parameters derived from the individual estimates, grouped per inter-comparison project. Inside the ellipses falls 80 % of the distribution.

ESDD
3, 935–977, 2012

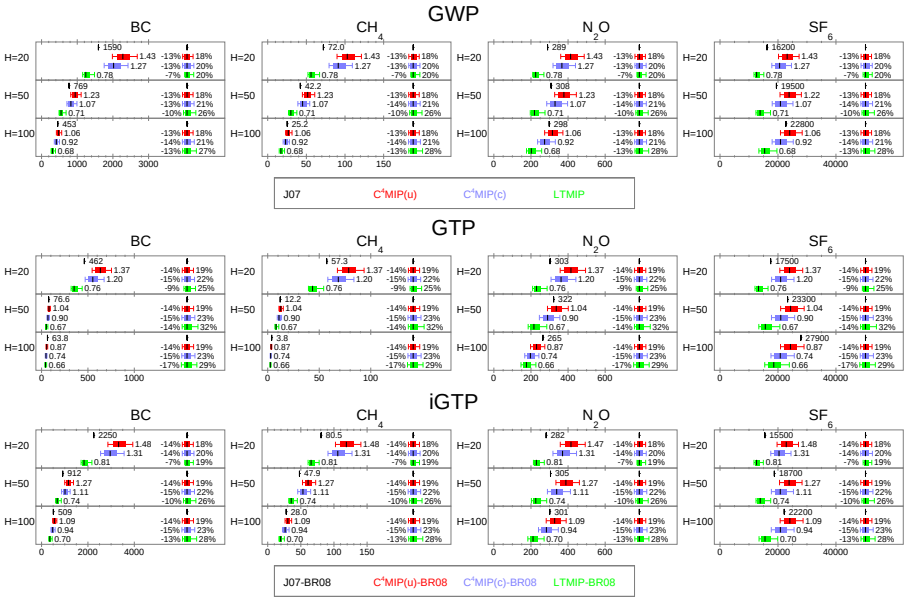

Fig. 3. Impact of spread in the CO_2 IRF on GWP, GTP and iGTP values for BC, CH_4, N_2O, and SF_6, for time horizons of 20, 50, and 100 yr. The values have been calculated using four different CO_2 IRFs: J07 (black), C^4MIP(u) (red), C^4MIP(c) (blue), and LTMIP (green). For the calculation of GTP and iGTP we additionally used the reference temperature IRF BR08. For every time horizon, the little black line (top) gives the value of the metric using the reference IRF – the value itself is indicated right of the little line. The left bars give the value of the metric using the three different IRFs: the bar indicates the 10-, 25-, 50-, 75-, and 90-percentile values of the metric (the 50-percentile value is indicated by a black line). The number indicates how much the median value (50-percentile, indicated in black) deviates from the reference value. The right bars indicate the spread with respect to the median value, where again the 10-, 25-, 75-, and 90-percentile values are represented. The numbers (in %) left and right of the bar indicate how much the 10- and 90-percentile value deviate from the median value.

ESDD
3, 935–977, 2012

The impact of model variation on emission metrics

D. J. L. Olivié and G. P. Peters

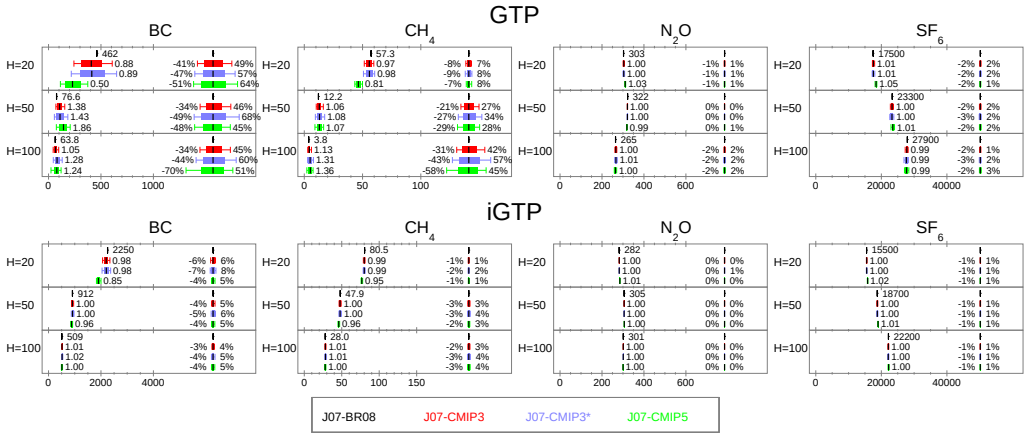

Fig. 4. Impact of spread in the temperature IRF on GTP and iGTP values for BC, CH_4, N_2O, and SF_6, for time horizons of 20, 50, and 100 yr. The values have been calculated using four different temperature IRFs: BR08 (black), CMIP3 (red), CMIP3*(blue), and CMIP5 (green). We have always used the J07 CO_2 IRF. For the explanation of the figure, see Fig. 3.

ESDD
3, 935–977, 2012

The impact of model variation on emission metrics

D. J. L. Olivié and G. P. Peters

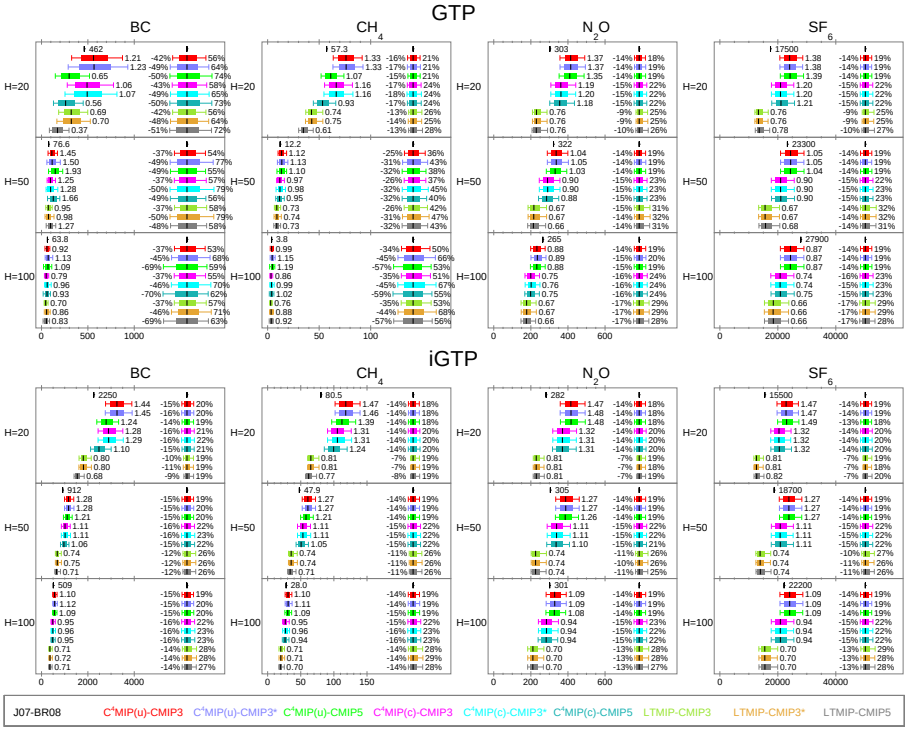

Fig. 5. Impact of spread in both CO_2 and temperature IRF on GTP and iGTP values for BC, CH_4, N_2O, and SF_6, for time horizons of 20, 50, and 100 yr. We used for the reference (black) the combination of the J07 CO_2 IRF and BR08 temperature IRF. The other cases are combinations of the three CO_2 IRFs (C^4MIP(u), C^4MIP(u), and LTMIP) and the three temperature IRFs (CMIP3, CMIP3*, and CMIP5). For the explanation of the figure, see Fig. 3.

ESDD
3, 935–977, 2012

The impact of model variation on emission metrics

D. J. L. Olivié and G. P. Peters